Seventh South African Conference on Computational and Applied Mechanics
SACAM10
Pretoria, 10−13 January 2010

A MEMS BASED VALVELESS MICROPUMP FOR BIOMEDICAL APPLICATIONS

Schalk W. van der Merwe[*,1], **Albert A. Groenwold**[*,2], **Philip W. Loveday**[†] **and G. D. Thiart**[*,3]

[*]Department of Mechanical and Mechatronical Engineering
University of Stellenbosch, Private Bag X1, Stellenbosch, 7602, South Africa,
[1]14130890@sun.ac.za, [2]albertg@sun.ac.za, [3]thiart@sun.ac.za.

[†]Sensor Science & Technology
CSIR Material Science & Manufacturing, Box 395, Pretoria, 0001, South Africa.
ploveday@csir.co.za.

Keywords: micropump, valveless, Jeffery-Hamel flow, Buckingham-Pi theorem

Abstract

The valveless micropump holds great potential for the biomedical community in applications such as drug delivery systems, blood glucose monitoring, and many others.

In this paper, we investigate the characteristics of a planar diffuser/nozzle based micropump using detailed computational fluid dynamics (CFD) analyses. The significant parameters are determined using the Buckingham-Pi theorem. In part based on this, the shape of the diffuser and the nozzle of the micropump, as well as the piezoelectric disc oscillation frequency, are selected for numerical investigation. The influences of the determined parameters on the flow rate of the micropump are then studied using three dimensional transient CFD analyses. The data from the CFD analyses are compared to velocity profiles from Jeffery-Hamel flow predictions in a wedge shaped channel. Significant similarities are found between the CFD data and the Jeffery-Hamel velocity profiles, especially near the exit of the diffuser where the flow is more developed.

Three different diffuser geometries are simulated at three different frequencies. The flow rate and direction of flow are shown to be highly sensitive to inlet and outlet diffuser shapes, with the absolute flow rate varying by as much as 200% for the geometrical perturbations studied. Entrance losses at both the diffuser inlet and nozzle inlet appear to dominate the flow resistance at extremely laminar flow conditions with an average Reynolds number of $Re_{average} \approx 500$.

1 Introduction

The first documented reports of a miniaturized pump or micropump date back to as early as 1975, e.g. see Tay [1]. Realizing the potential of the micropump in industries such as heat transfer, biomedicine and printing, researchers continued their investigations in later years. In 1993, Stemme and Stemme [2] designed and tested a valveless micropump based on the flow rectification properties of diffusers. The design proposed by Stemme and Stemme was simple and offered the advantage of low fabrication cost,

reduced wear, increased valve reliability and less clogging of the valves, which is prevalent in most passive check valve models.

Literature abounds with studies that emphasize the importance of geometric effects of the diffuser on the performance of micropumps, e.g. see Stemme and Stemme [2], Olsson *et al.* [3, 4], and Singhal *et al.* [5]. Since the diffuser forms an integral part of the performance of the micropump, many different geometries have previously been investigated. Among the diffuser geometries studied are conical [2, 6], pyramidal [3] and flat walled diffusers [3, 4]. The diffuser geometry is for the most part dependent on the type of fabrication processes available. However, under the same conditions, flat walled diffusers have been shown to be 10-80% shorter than conical diffusers for similar efficiency [7]. Due to its aforementioned qualities, the flatwalled diffuser is the subject of this study.

2 Diffuser and Nozzle Characteristics

The optimization of the diffuser is integral to the performance of the micropump, but little experimental data and few analytical expressions exists that describe pressure losses in the diffuser [8]. An exception is Runstadler *et al.* [9], but the data is predominantly for turbulent flows and not for laminar flow as is the case for micro-diffusers. Numerical and experimental results presented in the literature is case dependent. If however literature cases are combined with data from Runstadler *et al.* [9], this offers valuable insight into diffuser behavior.

Diffuser operation can be classified into four modes as depicted in Figure 1(a), depending on the diffuser geometry. The no-stall region occurs when flow is steady and viscous with no separation at the diffuser walls and diffuser performance is relatively good in this region. Transitory-stall is reached when flow is unsteady and pressure loss is a minimum. Bistable steady-stall flow occurs when the flow flip-flops between the diffuser walls and performance is poor in this region. Flow is said to be in the jet flow region when it separates completely from the diffuser walls and passes through at a near constant cross-sectional area [7].

Minimum pressure loss as depicted in Figure 1(a) is illustrated graphically in Figure 1(b) as an experimental study and provides information on the performance of the diffuser element. Although intended for very high Reynolds number flows, Figure 1(b) can be utilized to aid the design process and provide an estimate of parameter influences. However, it should be emphasised that the data presented in Figure 1(b) is at best a crude estimate and Wang *et al.* [10] and Jiang *et al.* [11] have provided data that suggested major differences when the Reynolds number approached Re ≤ 100.

A measure of the efficiency for the micro-diffuser is a dimensionless coefficient, called the diffuser pressure loss coefficient K_d [7], and is defined as [3, 4, 10, 11, 12]

$$K_d = \frac{\Delta p_d}{\frac{1}{2}\rho V_c^2} \,, \tag{1}$$

where ρ is the fluid density, V_c is the characteristic velocity of the flow and Δp_d is the pressure difference over the diffuser.

Similarly, K_n for a nozzle is defined as [5]

$$K_n = \frac{\Delta p_n}{\frac{1}{2}\rho V_c^2} \,, \tag{2}$$

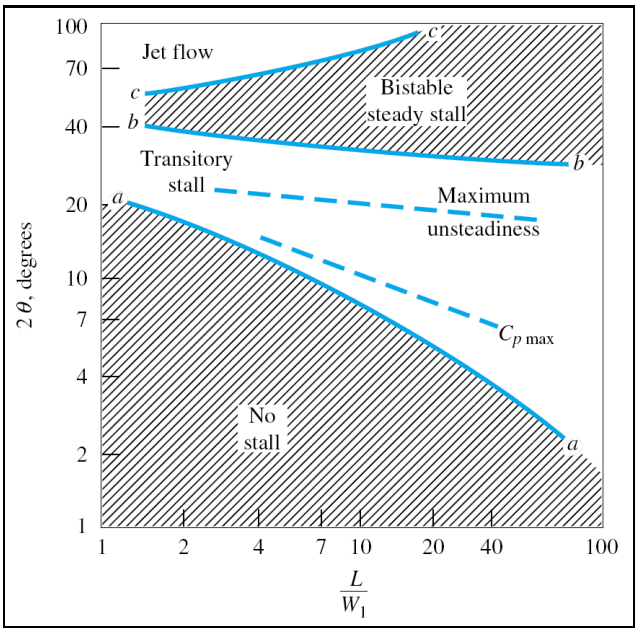

(a) Stability map of a typical diffuser [9].

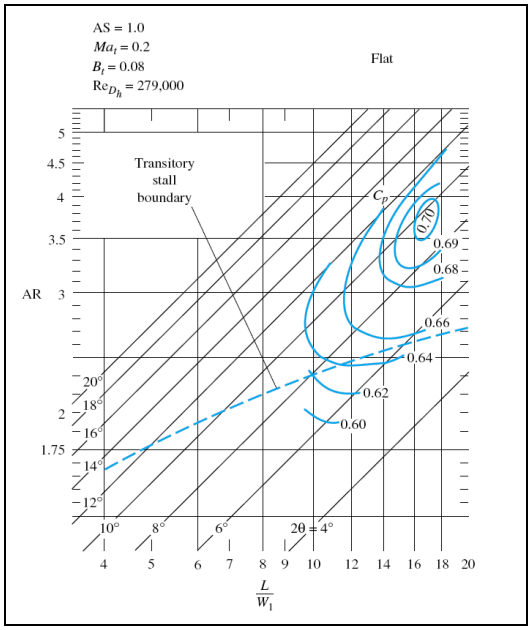

(b) Performance map of typical flat walled diffuser [9].

Figure 1: Typical performance and stability maps for diffusers.

where Δp_n = pressure difference over the length of the nozzle.

Pressure loss coefficients as defined in Equations (1) and (2) consist of three areas of pressure loss: $\Delta p_{d,en}$ – pressure losses due to sudden contraction at the entrance of the diffuser, Δp_d – pressure losses due to viscous flow in the expanding cross-section, and $\Delta p_{d,ex}$ – pressure losses due to sudden expansion at the exit of the diffuser.

The total pressure loss can then be written as

$$\Delta p_{d,total} = \Delta p_{d,en} + \Delta p_d + \Delta p_{d,ex} \ , \tag{3}$$

and using Equations (1) and (3), the total pressure loss coefficient for a diffuser can be written as

$$\begin{aligned} K_{d,total} &= K_{d,en} + K_d + K_{d,ex} \\ &= \frac{\Delta p_{d,en}}{\frac{1}{2}\rho V_c^2} + \frac{\Delta p_d}{\frac{1}{2}\rho V_c^2} + \frac{\Delta p_{d,ex}}{\frac{1}{2}\rho V_c^2} \\ &= \frac{\Delta p_{d,total}}{\frac{1}{2}\rho V_c^2} \ . \end{aligned} \tag{4}$$

Hence, for a given diffuser geometry, the pressure loss coefficient can be estimated from the pressure drop and the mean velocity at the neck of the diffuser. However, these equations are largely simplified and usually intended for use in conventional diffusers. Therefore determining the pressure drop inside the diffuser or $\Delta p_{d,total}$ requires a numerical or experimental approach.

The diffuser efficiency η_{nd} for a nozzle-diffuser element is defined as the ratio of the total pressure loss coefficient for flow in the nozzle direction to that for the flow in the diffuser direction [5], i.e.

$$\eta_{nd} = \frac{K_{n,total}}{K_{d,total}} \ . \tag{5}$$

Thus, η_{nd} should be greater than one to provide a net flow rate in the diffuser direction. If η_{nd} is equal to one there is no net flow rate due to equal pressure drop in both directions. When η_{nd} is smaller than one the net flow is in the nozzle direction.

3 Dimensional Analysis

The goal of the dimensional analysis is to determine a functional relationship between the various design parameters as depicted in Figure 2(b). Consider the parameters of the diffuser as given by

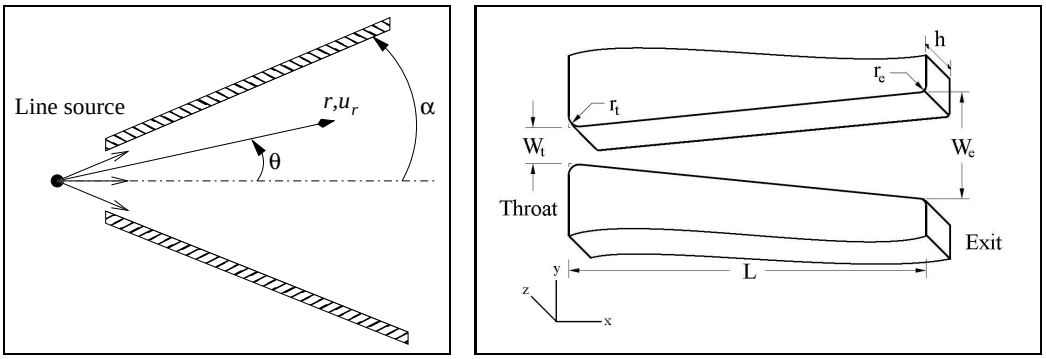

(a) Geometry and parameters of Jeffery-Hamel flow.

(b) A flat walled diffuser / nozzle element.

Figure 2: Diffuser parameters for Jeffery-Hamel flow and Buckingham Pi-theorem.

Figure 2(b), for which the functional relationship for the flow rate can be expressed as

$$\bar{Q} = F\left(\Delta p, f, \rho, \mu, L, h, W_t, W_e, r_t, r_e\right) , \tag{6}$$

where $\bar{Q}$ is the mean averaged flow rate, Δp is the applied differential pressure, f is the excitation frequency, μ is the fluid viscosity, L is the total length of diffuser, h is the depth of diffuser, W_t is the width of the throat of the diffuser, W_e is the width of the diffuser exit, r_t is the inlet radii for the throat of the diffuser, and r_e is the outlet radii for the exit of the diffuser.

The expression in (6) can be simplified using dimensional analysis. The method presented here was proposed in 1914 by Buckingham [13], and is now known as the Buckingham Pi-theorem. The theorem states that when a problem is written as a functional relationship, $Q_i = f(Q_1, Q_2, ..., Q_n)$ in terms of n dimensional variables, then these terms are physically relevant in the problem and are inter-related by an unknown dimensionally homogeneous set of equations. If r is the number of fundamental dimensions required to describe the n variables, the remaining $p = n - r$ variables can be expressed as p dimensionless and independent "Pi-groups". Thus any functional relationship of this form can be reduced to $\prod_i = \phi\left(\prod_1, \prod_2, ..., \prod_{n-r}\right)$.

For the problem as set out in (6) there will be $11 - 3 = 8$ independent dimensionless groups. The simplified equation will not be unique, and one possibility for this functional relationship is

$$\frac{\rho \bar{Q}}{\mu L} = F\left(\frac{\rho L^2 \Delta p}{\mu^2}, \frac{\rho L^2 f}{\mu}, \frac{W_t}{L}, \frac{W_e}{L}, \frac{h}{L}, \frac{r_t}{W_t}, \frac{r_e}{W_e}\right) , \tag{7}$$

assuming that the applied pressure Δp and the frequency of excitation f are properties of the piezoelectric disk and not the geometry of the micropump these parameters are not considered for this investigation. As the piezoelectric disk is not the focus of the research presented, the remaining parameters are W_t, W_e, L, h, r_t and r_e.

Using Figure 1(b) and data from [9], it is clear that the optimal performance for diffusers angles ranges from $5^\circ \leq 2\theta \leq 10^\circ$. From this an angle of $2\theta = 7.5^\circ$ and a dimension of $W_t = 80$ μm are selected for the design (which conforms with manufacturing capabilities). From these specified values and Figure 1(b), the maximum C_p is found at $L/W_t = 13.75$, which means an AR (area ratio) of W_e/W_t = 2.7.

As the depth h of the diffuser is a constant (planar diffuser) and fixed by manufacturing capabilities to 80 μm, the remaining variable parameters of Equation (7) are the inlet radii r_t and outlet radii r_e of the diffuser. The inlet and outlet radii of the diffuser are thus selected for further investigation.

4 Jeffery-Hamel flow in a wedge shaped region

Diffuser and nozzle flow is presented here in polar coordinates for a wedge shaped region. This work presented here is one specific numerical solution to Jeffery-Hamel flow, as presented by White [14].

When the flow is assumed to be purely radial the momentum equation is reduced to a third-order, non-linear ordinary differential equation. The problem, altough a boundary value problem, is solved numerically using Matlab's Runge-Kutta initial value problem solver i.e. `ode45`.

As depicted in Figure 2(a), the flow is considered in polar coordinates r and θ, generated by a line source at the origin as presented by White [14]. The flow in the diffuser is considered to be purely radial hence $u_\theta = 0$ and bounded by the sidewalls at $\theta = \pm\alpha$.

4.1 Analytical model derivation

The continuity equation in polar coordinates as given by [14]

$$\frac{1}{r}\frac{\partial}{\partial r}(ru_r) = 0 \, . \tag{8}$$

If u_r have a local maximum at $\theta = 0$, then a nondimensionalization for the problem is

$$\eta = \frac{\theta}{\alpha} \, , \tag{9}$$

and

$$f(\eta) = \frac{u_r}{u_{max}} \, . \tag{10}$$

The momentum equation in polar coordinates for $u_\theta = 0$ is given by [14]

$$\begin{aligned} u_r\frac{\partial u_r}{\partial r} &= -\frac{1}{\rho}\frac{\partial p}{\partial r} + \nu\left(\frac{\partial^2 u_r}{\partial r^2} + \frac{1}{r}\frac{\partial u_r}{\partial r} - \frac{u_r}{r^2} + \frac{1}{r^2}\frac{\partial^2 u_r}{\partial \theta^2}\right) \, , \\ 0 &= -\frac{1}{\rho r}\frac{\partial p}{\partial \theta} + \frac{2\nu}{r^2}\frac{\partial u_r}{\partial \theta} \, . \end{aligned} \tag{11}$$

Pressure is eliminated by cross differentiation and introducing the variables from Equation (9) and (10). The result is a third-order non-linear ordinary differential equation for the velocity profile f of the form

$$f''' + 2Re\alpha f f' + 4\alpha^2 f' = 0 \, , \tag{12}$$

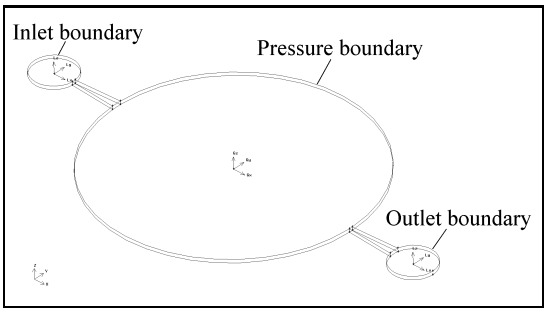

Figure 3: Three dimensional layout of the micropump model.

where $Re = u_r r\alpha/\nu$ is the characteristic Reynolds number for the flow presented. Flow is assumed to be symmetric and a no slip boundary condition is applied at the walls. As mentioned u_{max} is at $\theta = 0$. The initial and boundary values can thus be summarized by

$$\begin{aligned} f(+1) = f(-1) = 0\ , \\ f(0) = 1\ , \\ f^{'}(0) = 0\ . \end{aligned} \tag{13}$$

Equation (12), combined with initial and boundary values from (13), is solved numerically using Matlab's Runge-Kutta solver i.e `ode45` as illustrated by [15]. Equation (12) is solved for a range of $Re\alpha$ values. Data from the CFD simulations are compared to the predicted Jeffery-Hamel velocity distributions and are graphically illustrated in Figures 5(b), 6(b) and 7(b). The solutions are plotted for the $Re\alpha$ value at the exit of the diffusers, where the flow is more developed.

5 Numerical simulations

A two-dimensional, steady state model of the micro-diffuser was solved to test the mesh dependancy. Mesh bi-section was used to refine the mesh and the optimum mesh settings were extrapolated to the three-dimensional model.

The CFD solver used for all simulations is Fluent 6.3.26. A pressure based solver is chosen and the SIMPLE pressure-velocity coupling scheme is selected for the analysis. The second order upwind numerical scheme is used for the momentum equation calculations. Small flow volumes is expected, the absolute convergent criteria is therefore set to 1×10^{-12} and the laminar viscous model is selected. Fluid properties of water at $20\,^{\circ}\mathrm{C}$ is used for the fluid.

A three-dimensional model is simulated with three different inlet and outlet radii configurations as depicted by Figure 4. All models are solved at an excitation frequency of 1 kHz and the time step is set to Δt = 0.01 ms. The model has 400 000 cells and is solved on a parallel computing Linux cluster. A model similar to the one depicted in Figure 3 is used in the numerical investigation. A sinusoidal pressure at 1 kHz is applied to the pump chamber and the outlet flow rates are calculated. Velocity vectors are recorded on three depths in the diffuser, at 40 μm, 25 μm and 5 μm.

- **Sharp edged diffuser/nozzle configuration**

  In this model the diffuser inlet and nozzle inlet edge has angles approaching 90° as depicted in Figure 4(a). The resulting flow rates are plotted in Figure 5(a) and the comparison between the predicted Jeffery-Hamel velocity profiles and the CFD data are plotted in 5(b).

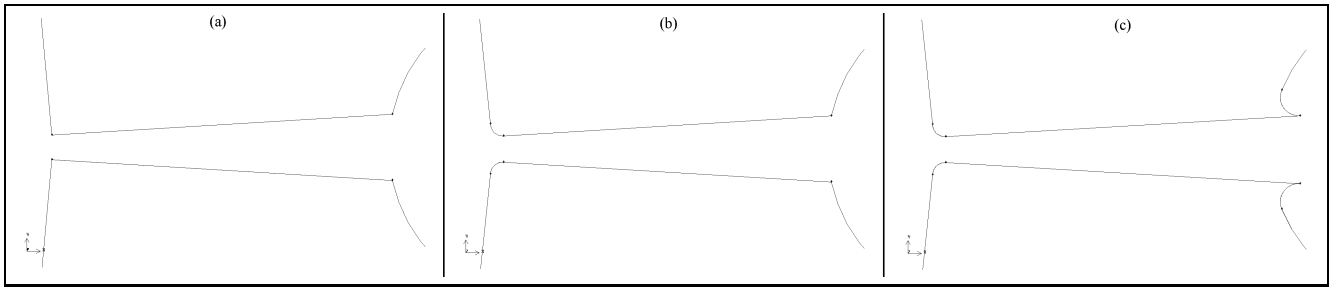

Figure 4: (a) A two-dimensional diffuser model with sharp diffuser and nozzle inlet radii. (b) A two-dimensional diffuser model with rounded diffuser inlet edge and sharp nozzle inlet edge. (c) A two-dimensional diffuser model with rounded diffuser inlet edge and sharpened nozzle inlet edge.

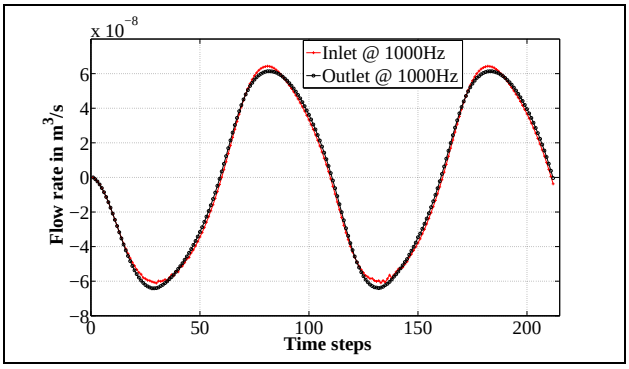

(a) Inlet and outlet flow rates for the sharp edged diffuser nozzle configuration exited at 1 kHz for 2 ms and with $\Delta t = 0.01$ ms.

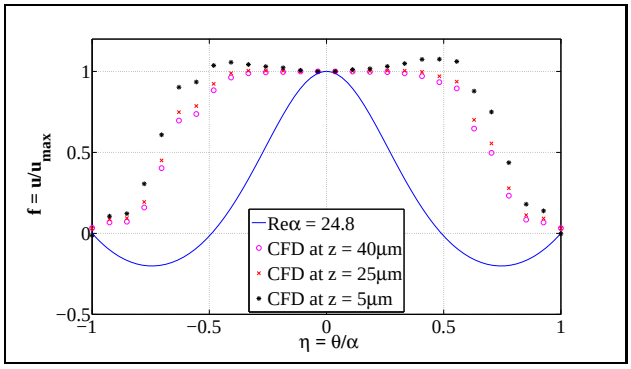

(b) A comparison between the predicted Jeffery-Hamel velocity profiles and the calculated CFD velocity vectors at the exit of the diffuser and at three depths in the diffuser for the sharp edged diffuser nozzle model.

Figure 5: Results for the sharp diffuser and nozzle inlet configuration (see Figure 4(a)).

- **Round edged diffuser/nozzle configuration**

  This model has a rounded inlet edge, r_t = 40 μm, for diffuser flow and a sharp inlet edge, angles approaching $90°$, for the nozzle flow as depicted in Figure 4(b). The resulting flow rates are plotted in Figure 6(a) and the comparison between the predicted Jeffery-Hamel velocity profiles and the CFD data are plotted in 6(b).

- **Round edged diffuser and sharpened edge nozzle configuration**

  This model has a rounded inlet edge, r_t = 40 μm, for diffuser flow and a sharpened inlet edge, angles approaching $180°$, for the nozzle flow as depicted in Figure 4(c). The resulting flow rates are plotted in Figure 7(a) and the comparison between the predicted Jeffery-Hamel velocity profiles and the CFD data are plotted in 7(b).

6 Results and Discussion

Considering Figures 5(a), 6(a) and 7(a), the nett flow rate $\bar{Q}$ can be calculated as

$$\bar{Q} = \sum Q_{outlet} - \sum Q_{inlet} \ , \tag{14}$$

which means that if $\bar{Q} \leq 0$, the pump direction is in the diffuser direction. If however $\bar{Q} \geq 0$, the pump direction is in the nozzle direction. The inlet and outlet curves of Figures 5(a), 6(a) and 7(a) are integrated numerically and calculated as in Equation (14).

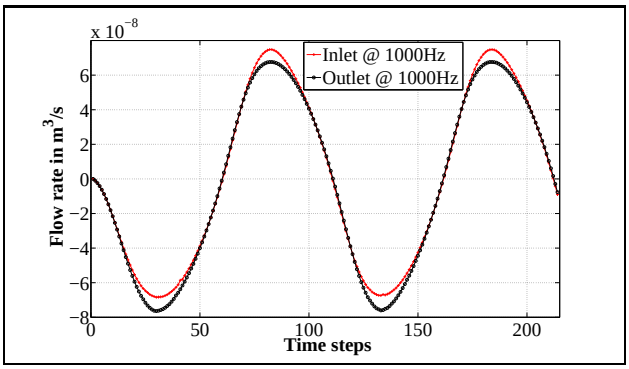

(a) Inlet and outlet flow rates for the rounded diffuser inlet and sharp nozzle inlet configuration exited at 1 kHz for 2 ms and with $\Delta t = 0.01$ ms.

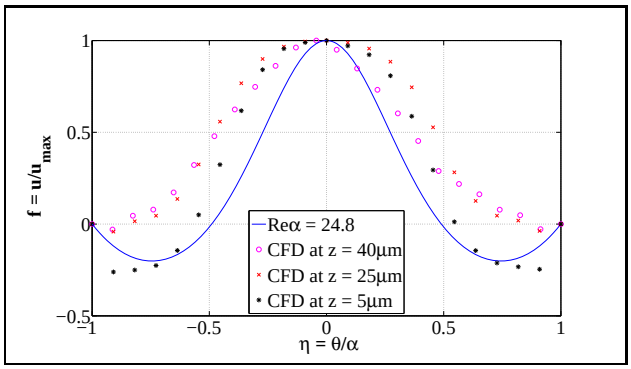

(b) A comparison between the predicted Jeffery-Hamel velocity profiles and the calculated CFD velocity vectors at the exit of the diffuser and at three depths in the diffuser for the rounded diffuser inlet edge and sharp nozzle inlet edge model.

Figure 6: Results for the rounded diffuser inlet model (see Figure 4(b))

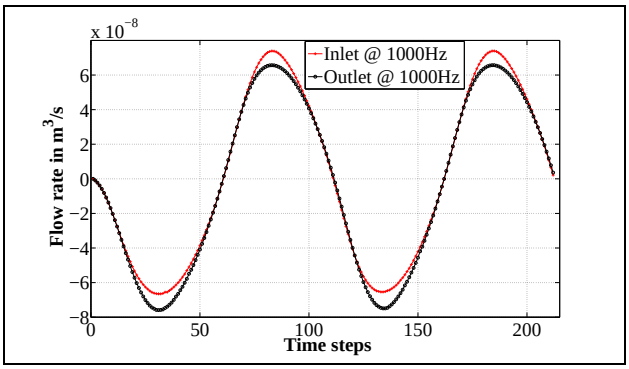

(a) Inlet and outlet flow rates for the rounded diffuser inlet and sharpened nozzle inlet configuration exited at 1 kHz for 2 ms and with $\Delta t = 0.01$ ms.

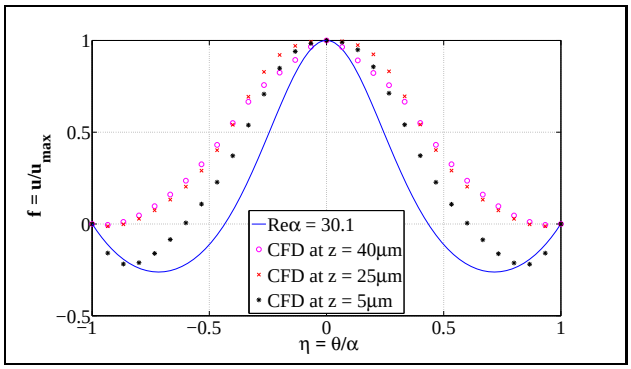

(b) A comparison between the predicted Jeffery-Hamel velocity profiles and the calculated CFD velocity vectors at the exit of the diffuser and at three depths in the diffuser for the rounded diffuser inlet edge and sharpened nozzle inlet edge model

Figure 7: Results for the rounded diffuser inlet and sharpenend nozzle inlet configuration (see Figure 4(c)).

- **Sharp edged diffuser/nozzle configuration**

  Analysing the data from Figure 5(a) with Equation (14) the nett flow rate $\bar{Q}$ of the pump is calculated as 3679 μl/min. As $\bar{Q} \geq 0$, it shows the nett flow direction to be in the nozzle direction. The flow rate is reversed from what was expected. This result illustrates the high entrance losses associated with very low Reynolds number flows ($Re_{max} \approx 900$). Even with large flow separation from the sidewalls, the inlet losses $K_{d,en}$ dominate the flow resistance at all simulated frequencies.

  From Figure 5(b) it is clear that the flow is never fully developed and large velocity gradients at the diffuser wall contribute to large shear forces. These large shear forces contribute to the already high flow resistance in the diffuser direction. It is also observed that there is negligible black flow in the diffuser and there is very little comparison to the Jeffery-Hamel velocity distribution. Since the Jeffery-Hamel flow prediction assumes fully developed flow, discrepancies between the data and the Jeffery-Hamel flow prediction is expected.

- **Round edged diffuser/nozzle configuration**

  Analysing the data from Figure 6(a) with Equation (14) the nett flow rate $\bar{Q}$ of the pump is calculated as -8635 μl/min. As $\bar{Q} \leq 0$, it shows the nett flow direction to be in the diffuser direction. The rouned inlet for the diffuser illustrates the effect of the entrance losses at low Reynolds numbers. Compared to the sharp diffuser inlet model the absolute flow rate is improved by more than 110% on the absolute flow rate. The flow in this model is in the diffuser direction opposed to the nozzle direction as is the case in the sharp edge model.

  From Figure 6(b) it is clear that the flow is more developed than that of the sharp edged model. Minor backflow is also observed on all three depths of the diffuser and contributes to a decreased flow resistance in the diffuser direction. The velocity vectors from the CFD data are also closer to the predicted Jeffery-Hamel velocity distribution than the sharp edged model's.

- **Round edged diffuser and sharpened edge nozzle configuration**

  Analysing the data from Figure 7(a) with Equation (14) the nett flow rate $\bar{Q}$ of the pump is calculated as -11460 μl/min. As $\bar{Q} \leq 0$, it shows the nett flow direction to be in the diffuser direction. The sharpened inlet for the nozzle illustrates the effect of the entrance losses at low Reynolds numbers. Compared to the round diffuser inlet model the flow rate is improved by more than 30%. This improvement on the flow rate can be attributed to the increased losses at the entrance in the nozzle direction as depicted by Figures 8(a) and 8(b).

  From Figure 7(b) it is observed that the flow is more developed than that of the rounded edged model. Major backflow is also observed near the bottom of the diffuser and contributes to a reduced flow resistance in the diffuser direction. The velocity vectors from the CFD data are also closer to the predicted Jeffery-Hamel velocity distribution than the sharp edged model's.

7 Conclusion

The data analysed shows the dependency of the flow direction on variables such as inlet and outlet radii. This dependency can be explained by large losses at the diffuser entrance due to extreme velocity gradients in this area. This effect is illustrated in Figures 8(a) and 8(b).

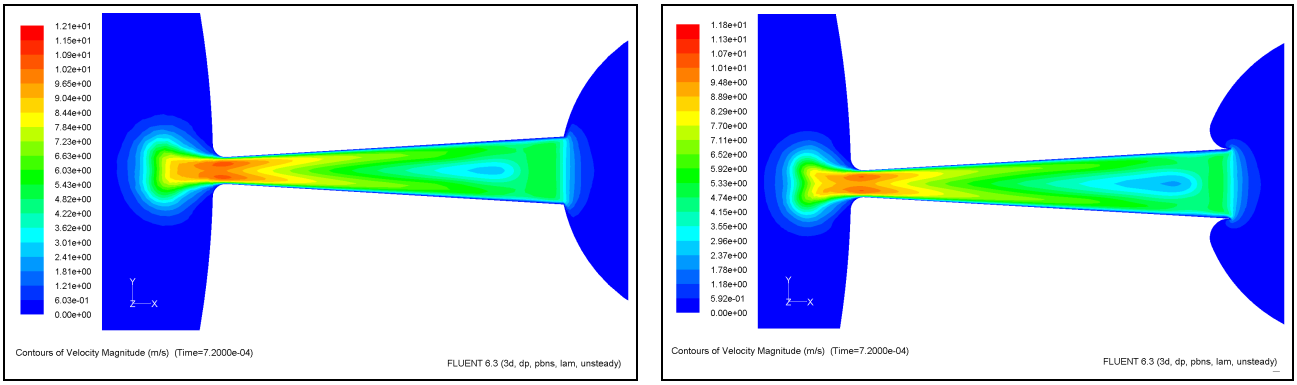

(a) Velocity contour plot of the nozzle flow for the sharp nozzle inlet edge model.

(b) Velocity contour plot of the nozzle flow for the sharpened nozzle inlet edge model.

Figure 8: Velocity magnitude distribution plots illustrating the higher velocity gradients at the entrance of the sharpened nozzle inlet edge model.

By implementing a rounded diffuser inlet throat, where the velocity gradients are large, the efficiency of the micropump is increased (as seen by comparing Figures 5(a) and 6(a)). The nett flow rate is further increased by adding sharper inlet edges to the nozzle flow direction, which increases flow resistance in the nozzle direction by amplifying inlet losses. This effect becomes visible by comparing Figures 5(a) and 7(a). Compared to the round diffuser inlet model the flow rate is improved by more than 30%. The effect of the alterations on the respective radii have increased the sharp edged model's absolute flow rate by more than 200%.

At low Reynolds numbers $|Re_{average}| \approx 500$, entrance losses appear to dominate the flow direction in both diffuser and nozzle direction.

References

[1] F.E.H. Tay, editor. *Microfluidics and BioMEMS Applications*. Kluwer Acedemic Publishers, 2002.

[2] E. Stemme and G. Stemme. A valve-less diffuser / nozzle based fluid pump. *Sensors and Actuators*, A39:159–167, 1993.

[3] A. Olsson, G. Stemme, and E. Stemme. Numerical and experimental studies of flat-walled diffuser elements for valve-less micropumps. *Sensors and Actuators*, 84:165–175, 1998.

[4] A. Olsson, G. Stemme, and E. Stemme. Diffuser-element design investigation for valve-less pumps. *Sensors and Actuators*, A 57:137–143, 1996.

[5] V. Singhal, S.V. Garimella, and J.Y. Murthy. Low reynolds number flow through nozzle-diffuser elements in valveless micropumps. *Sensors and Actuators*, A 113:226 – 235, 2003.

[6] M. Aumeerally. Analytic model derivation of microfluidic flow for mems virtual-reality cad. Master's thesis, School of Information and Communication Technology, Faculty of Engineering and Information Communication Technology, Griffith University, Queensland, Australia, 2004.

[7] F.M. White. *Fluid Mechanics*. McGraw-Hill international Editions, 1986.

[8] A. Olsson. Valve-less diffuser pumps for liquids. Master's thesis, Instrumentation Laboratory, Department of Signals, Sensors and Systems, Royal Institute of Technology, Stockholm, 1996.

[9] P.W. Runstadler, F.X. Dolan, and R.C. Dean. Diffuser data book. Technical report, Creare Inc. Science and Technology, 1975.

[10] Y.C. Wang, J.C. Hsu, P.C. Kuo, and Y.C. Lee. Loss characteristics and flow rectification property of diffuser valves for micropump applications. *International Journal of Heat and Mass Transfer*, 52:328–336, 2009.

[11] X.N. Jiang, Z.Y. Zhou, X.Y. Huang, Y. Li, Y.Yang, and C.Y. Liu. Micronozzle/diffuser flow and its application in micro valveless pumps. *Sensors and Actuators*, A 70:81–87, 1998.

[12] W. Wang and S.A. Soper. *Bio-MEMS Technologies and Applications*. CRC Press, Taylor & Francis Group, 2007.

[13] E. Buckingham. On physically similar systems: Illustrations of the use of dimensional equations. *Phys. Rev.*, 4:345–376, 1914.

[14] F. M. White. *Viscous Fluid Flow*. McGraw-Hill, 2006.

[15] G. Lindfield and J. Penny. *Numerical Methods using Matlab®*. Prentice Hall, 2000.